Patterns and Symmetries in Spiking Neural Networks

Victoria Zhang

Phillips Academy

Andover, MA 01810, USA

Dr. Bolun Chen

Brandeis University

Waltham, MA 02453, USA

PATTERNS AND SYMMETRIES IN SPIKING NEURAL NETWORKS

Victoria Zhang

ABSTRACT

Inspired by recent progress in computational neuroscience and artificial intelligence, this paper explores rich temporal patterns in networks of neurons that communicate via electric pulses known as spikes. In particular, we describe the attractors in small circuits of spiking neurons with different symmetries and connectivities. Using methods developed in the theory of dynamical systems, we extend an analytical approach to capture the phase-locked states and their stability for a general N-cell system. We then systematically explore attractors in reduced state spaces via Poincaré maps for both all-to-all coupled and star-like coupled networks. We identify a sequence of bifurcations when the coupling strengths vary from inhibition to excitation. Moreover, using high-precision numerical simulations, we find two novel states in star-like networks that are unobserved in all-to-all networks: the death of oscillation for inhibitory coupling and quasi-periodic behaviors for excitatory coupling. Our results elucidate the interplay between dynamical patterns and symmetries in the building blocks of real networks. Furthermore, as self-sustained oscillations with pulsatile couplings are ubiquitous, our analysis may clarify understanding of not only neural dynamics but also other pulse-coupled oscillator systems such as non-linear electric circuits, wireless sensor networks, and self-organizing chemical reactions.

Keywords Leaky Integrate-and-Fire Neuron, Network Topology, Death of Oscillation, Cluster Synchrony

Table of Contents

1 Introduction

Due to a balance between energy supply and dissipation, many nonlinear systems in nature exhibit self-sustained oscillations, such as flashing fireflies [1], bursting pacemaker cells [2], chirping crickets [3], and chorusing tree frogs [4]. In particular, nerve cells or neurons in the human brain can elicit periodic pulses in their membrane potential. These periodic pulses are known as spikes, with which neurons communicate and transmit information. Spiking neurons, or more precisely, their dynamical patterns, are the basic element of motor-control [5, 6], perception [7], memory consolidation and retrieval [8], and other high-level cognitive functions [9]. Many works [10, 11, 12] have demonstrated the computing capability of a network of such spiking neurons. Others have suggested neural-inspired algorithms [13, 14, 15] to improve the performance of artificial neural networks (ANN). Recent years have seen a resurgence in the study of ANN and its broad applications to scientific research and the industry [16]. A deep understanding of neural dynamics is therefore undoubtedly of a broad interest in physics, neuroscience, and artificial intelligence.

From a mathematical perspective, a single neuron is a multi-dimensional nonlinear dynamical system [17]. Periodic spikes in the membrane potential correspond to stable limit cycles in the state space, where asymptotic trajectories approach a closed orbit in the state space. One may use a phase-like variable to describe the neuron's state on the limit cycle [18]. Small perturbations only slightly deform the limit cycle and shift the phase. Thus, unlike a simple harmonic oscillator, the rigidity of the limit cycle renders a neuron adaptive to driving stimuli by adjusting its phase. Entrainment can occur when the cell receives external currents or inputs from other cells. Because a neuron in a network often makes contact with multiple neurons via synapses, rich dynamics emerge as a result of mutual entrainment [19].

It is well known that a network's dynamics can be largely affected by its connectivity, which is described by the adjacency matrix of the underlying graph [20, 21]. If the adjacency matrix is invariant under a sub-group of permutation of nodes, then the network is said to have a certain symmetry, under which the equations of motion of involved nodes stay unchanged. It implies that the invariant nodes are indistinguishable if they follow the same dynamics (they form a cluster). Indeed, earlier works [22, 23, 24, 25] established a beautiful link between the symmetry of a network and the clustered states (synchronous patterns) that can exist. But existence of clustered states does not necessarily guarantee stability. It is the dynamical equations that determine which states are stable [26] and that can be easily observed in numerical simulations or experiments.

And as for spiking neurons, the inter-neuronal synaptic coupling plays a decisive role. Depending on the type of the synapse (excitatory or inhibitory) as well as its activation speed, a network of spiking neurons can exhibit a multitude of patterns, such as full synchrony [27, 28], clustered synchrony and quasi-periodic oscillations [29], and an asynchronous splay state [30]. In these works, the authors assumed an all-to-all coupled neural network (shown in Figure 1) which has the most symmetry. A natural question therefore arises: what patterns can a network exhibit if the graph has less symmetry?

In this paper, we address this question by considering identical spiking neurons coupled in a star-like network as shown in Figure 2. In this simple but non-trivial case, a central hub interacts simultaneously with multiple subordinate cells. As information is transferred among local units, this structure acts as a building block (a motif) of large networks, and can be found in many real-world systems such as superconducting junction arrays [31], computer networks [32], and mammalian brains [33].

Specifically, we model a neuron as a leaky integrate-and-fire (LIF) oscillator, a widely-used model in neuroscience and applied mathematics. We extend an analytical approach developed in [34] to capture the phase-locked states and their stability for N coupled neurons as an analytic function.

Using high-precision numerical integration, we next systematically explore attractors in the reduced state space via Poincaré maps for both all-to-all coupled and star-like coupled networks. For a star-like network, we obtain phase diagrams of attractors as a function of the synaptic time constant. We also find that there exists a sequence of bifurcations when the coupling strengths vary from inhibition to excitation. For instance, in the star-like network, neurons with fast and excitatory synapses exhibit quasi-periodic behaviors. This novel state is absent in the all-to-all network and is due in part to the unique connectivity of the graph.

The rest of the paper is organized as follows: we introduce the mathematical model in Section 2 and Poincaré maps as a dimensional reduction approach in Section 3. The aforementioned analytic function for determining the stability of phase-locked states is derived and studied in Section 4. Next, in Section 5, we thoroughly explore the attractors in an all-to-all network of three and four neurons and in a star-like network of four neurons. Finally, in Section 6, we briefly summarize our results and discuss directions for future research.

2 Leaky Integrate-and-Fire Model

We begin by introducing the leaky integrate-and-fire (LIF) neural model.

The dynamics of a network of N spiking neurons are described by the following equations

$$\dot{x_i} = a_i - x_i + \sum_{j=1}^{N} K_{ij} s_j(t), \qquad i = 1, ..., N$$

$$\dot{s_i} = \alpha(-s_i + b_i), \qquad \dot{b_i} = -\alpha b_i. \tag{1}$$

Here, $x_i \in [0, 1]$ represents the normalized membrane voltage of the ith individual oscillator; s_i is the synaptic current of the ith individual oscillator; and b_i is introduced as an auxiliary variable. Moreover, $a_i > 1$, $\alpha > 0$, and $K_{ij} \in \mathbb{R}$ are constant parameters. The overdots denote differentiation with respect to time t. Thus $\dot{x_i} \equiv dx_i/dt$. The condition $a_i > 1$ ensures that firing occurs in the absence of coupling. α is the synaptic time constant and determines the shape of emitted pulses when an oscillator fires. Finally, K_{ij} measures how strongly the ith oscillator is coupled with the jth oscillator. $K_{ij} > 0$ corresponds to excitatory coupling, whereas $K_{ij} < 0$ corresponds to inhibitory coupling.

Firings occur when one or more of the variables x_i reaches the threshold $x_i = 1$. At this instance, x_i is reset to 0 and b_i is augmented by α. Equivalently, if oscillator i fires at time t_0, $s_i(t)$ is then augmented by the function $\phi(t - t_0)$, where $\phi(t)$ is an $\alpha-$function defined as

$$\phi(t) = \alpha^2 t e^{-\alpha t}.$$

In between firings, $s_i(t)$ obeys the ODE

$$\ddot{s_i} + 2\alpha\dot{s_i} + \alpha^2 s_i = 0.$$

Therefore, $s_i(t)$ follows the form $(A + Bt)e^{-\alpha t}$ and decays to 0 in the absence of firing. However, because $a_i > 1$, firings inevitably occur; otherwise, $s_i(t)$ would decay to 0, but then the ith oscillator would reach the threshold in finite time [29].

As mentioned in Section 1, we will focus on networks with all-to-all coupling and star network coupling. All-to-all coupled systems are systems in which each oscillator is coupled with every other oscillator. Star network coupled systems, in contrast, consist of a central oscillator to which

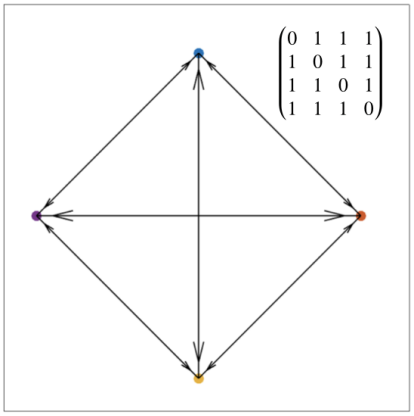

Figure 1: Schematic diagram of all-to-all coupled systems.

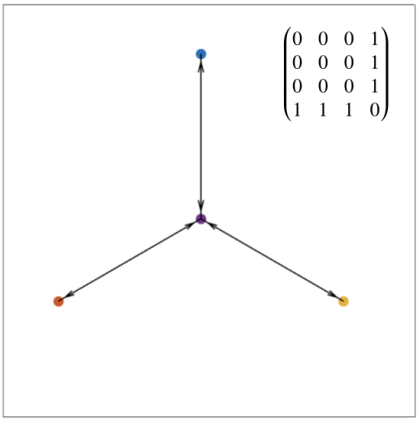

Figure 2: Schematic diagram of star network coupled systems.

every other oscillator in the system is coupled with. These two connectivity matrices are depicted schematically in Figures 1 and 2, in which arrows represent a nonzero coupling strength.

Finally, note that for a system with N identical oscillators with uniform all-to-all coupling, we can simplify (1) into

$$\dot{x_i} = a_i - x_i + Ks, \qquad i = 1, ..., N$$

$$\dot{s} = \alpha(-s + b), \qquad \dot{b} = -\alpha b \tag{2}$$

where $s = \sum_{j=1}^{N} s_j(t)$ and $b = \sum_{j=1}^{N} b_j(t)$.

Figure 3 shows the behavior of x and s of an LIF neuron. The graphs of x versus t illustrate that a neuron exhibits periodic, self-sustained oscillations. The graphs of s versus t plotted for two different values of α illustrate how α determines the shape of emitted pulses when a neuron fires.

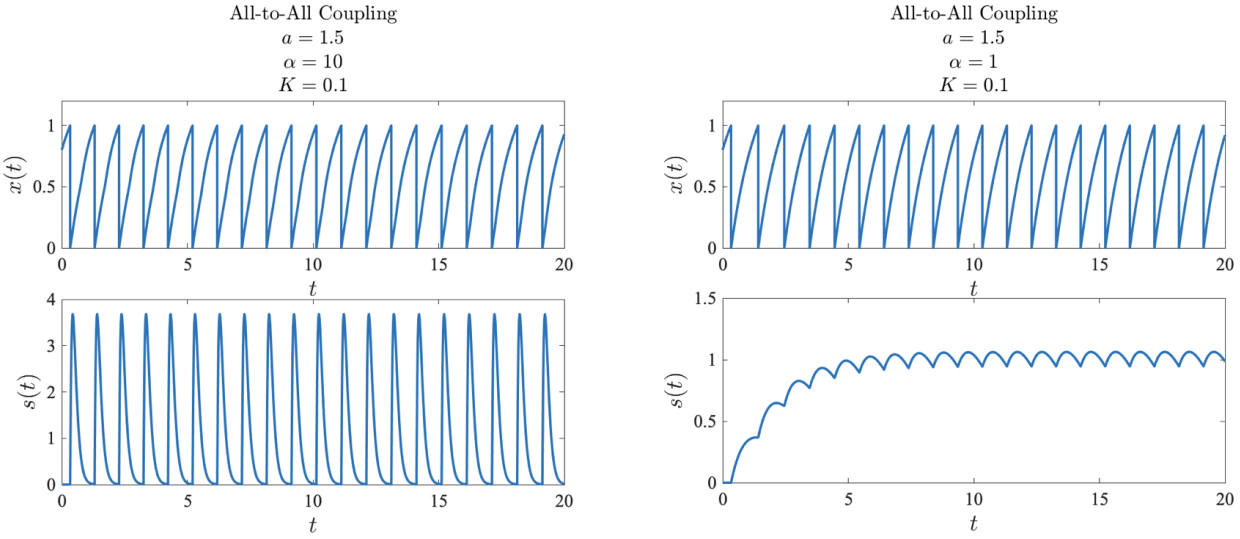

Figure 3: Evolutions of x and s of an LIF neuron with both fast ($\alpha = 10$) and slow ($\alpha = 1$) synapses.

3 Dimensional Reduction

Following [29] and [30], we utilize a Poincaré map to transform the continuously evolving systems described in Section 2 into discrete dynamical systems in state spaces of one fewer dimension. Our methodology is as follows: immediately after a selected oscillator fires, we plot the normalized action potentials of the other oscillators in the system. Without loss of generality, we focus on initial conditions in the fundamental domain $\mathbf{X_0}$ — which is an open set in which the variables $x_1, ..., x_{N-1}$ are distinct and have the same ordering [29] — defined by

$$0 = x_N \leq x_{N-1} \leq ... \leq x_1 < 1. \tag{3}$$

The geometry of the domain is an $N-1$-fold torus T^{N-1} (the full state space is T^N). Therefore, an $N = 3$ system reduces to a trajectory on the torus T^2, represented as a unit square. Similarly, an $N = 4$ system is represented on a unit cube. The boundaries of the fundamental domains consist of cluster synchrony states, in which two or more of the x_i's are identical and are invariant under the dynamics [29]. In other words, cluster synchrony corresponds to when 2 or more cells fire in synchrony.

Figures 4 - 8 show five solution states as Poincaré maps and as schematic diagrams, if applicable, for all-to-all coupled networks. In each of these figures, we used cell 1 to create a Poincaré section. Figures 4 - 6 showcase different cluster synchrony states in T^3, which are steady and time-evolving solutions. Here, a "3-1 cluster synchrony" means that 3 of the 4 cells are synchronized. Similarly, a "2-1-1 cluster synchrony" means that 2 of the cells are synchronized, and all other cells fire anti-synchronously with each other. Figure 7 shows the asynchronous splay state solution in T^2, where the trajectory reaches a final fixed point. Figure 8 shows the limit cycle solution on T^2, where the trajectory approaches a single and isolated closed loop. Note that color indicates the flow of time, starting with red, then orange, yellow, green, and so on.

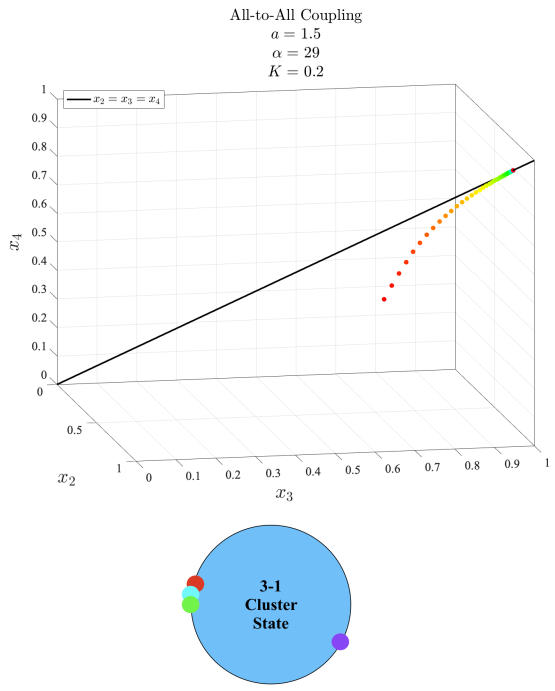

Figure 4: 3-1 Cluster synchrony; cells 2-4 synchronized.

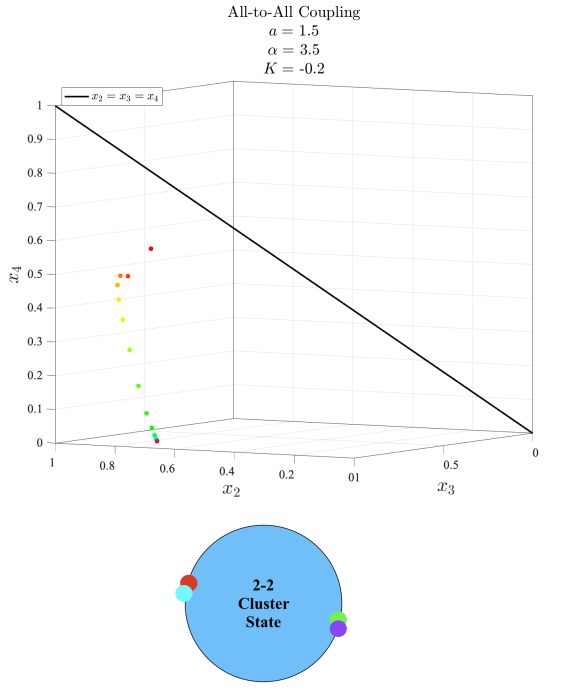

Figure 5: 2-2 Cluster synchrony; sychronized clusters of cells 1 and 4, and cells 2 and 3.

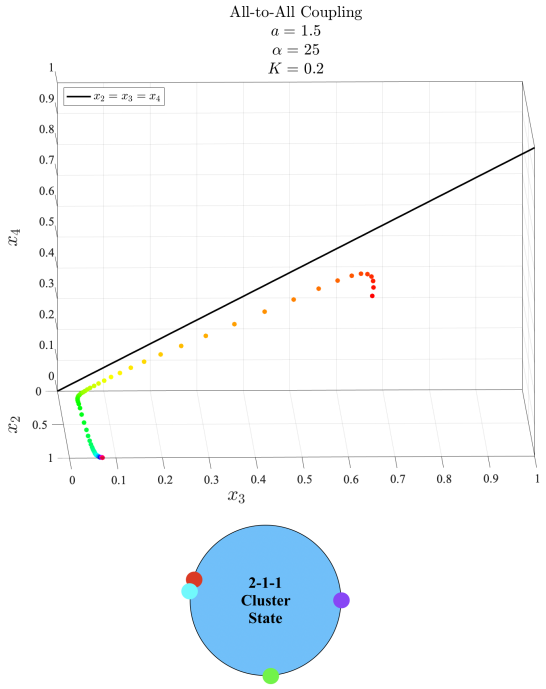

Figure 6: 2-1-1 Cluster synchrony, with cells 1 and 4 synchronized. This particular 2-1-1 cluster synchrony happens to be very close to 3-1 cluster synchrony.

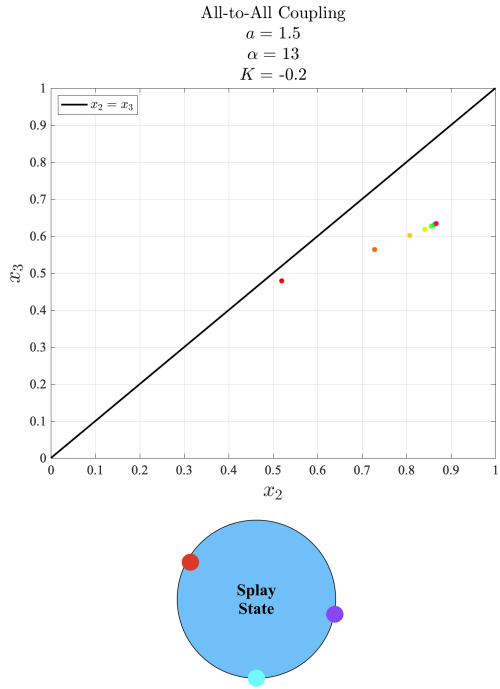

Figure 7: Splay state solution, where the trajectory reaches a final, fixed point.

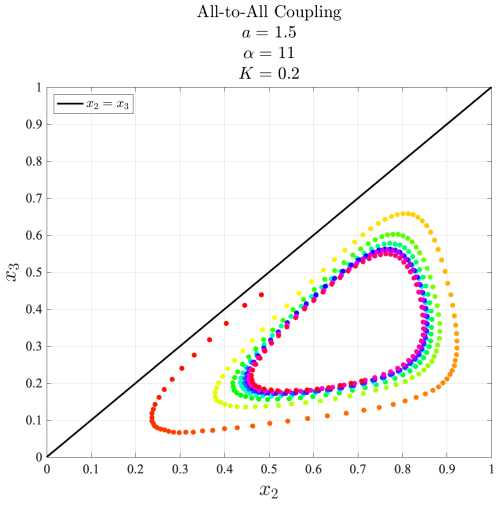

Figure 8: Limit cycle solution, a isolated closed trajectory.

4 An Analysis of Phase-Locked Solutions

In this section, we develop an analytic framework to examine phase-locked solutions in all-to-all coupled systems. A phase-locked state can be described as follows: each cell fires periodically with same period T and at a constant phase difference measured relative to the first cell. In other words, if the kth cell fires at a time $t_{s,k}$ and the first cell fires at a time $t_{s,1}$ where $t_{s,k} < t_{s,1}$, then the phase difference $\phi_{s,k} = \dfrac{t_{s,1} - t_{s,k}}{T}$ is constant. A phase-locked state is shown schematically in Figure 9.

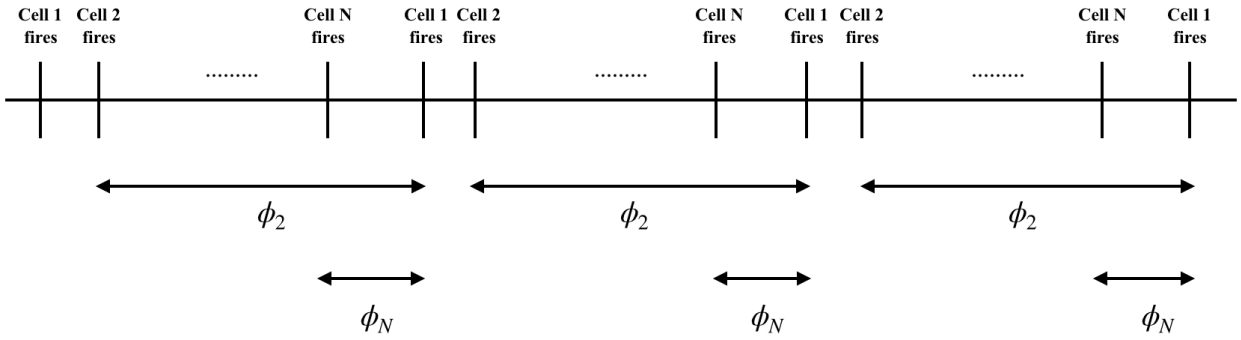

Figure 9: Schematic of an N-cell phase locked state.

Given a coupling matrix, we can define a function that captures the phase-locked states as a scalar function. Following the methodology introduced in [34], we extend their work to three cell systems and to the general N-cell system.

4.1 A Review of Two-Cell Systems

We start by reviewing the case of two identical coupled oscillators, studied in [34]. We consider cases in which the two cells reach a phase-locked state. Suppose that cell 1 fires periodically at t_s of the form $nT = \{\dots, -T, 0, T, \dots\}$ with $n \in \mathbb{N}$. Consequently, the input to cell 2 at $t = \theta T$, where θ is a fraction of the period T and $0 < \theta < 1$, is

$$s_{1\to 2}\left(\theta T\right) = s_T(\theta)$$

where

$$s_T(\theta) = \sum_{n=-\infty}^{0} \phi((\theta - n)T) = T\alpha^2 e^{-\alpha\theta T} \frac{\theta\left(1 - e^{-\alpha T}\right) + e^{-\alpha T}}{\left(1 - e^{-\alpha T}\right)^2}.$$

Note that our expression for s_T differs by a factor of K from [34]. Outside of the range $0 < \theta < 1$, $s_T(\theta)$ is defined as a periodic function:

$$s_T(\theta - 1) = s_T(\theta) = s_T(\theta + 1).$$

With cell 2 firing at $t = (n - \phi_2)T$, the input to cell 1 is

$$s_{2\to 1}\left(\theta T\right) = s_T(\theta + \phi_2).$$

Since cell 1 fires at $t = 0$, we have $x_1(0^+) = 0$. Here, $x_1(0^+)$ indicates the value of x_1 right after cell 1 has fired at $t = 0$. Integrating (2) yields

$$x_1(T) = 1 = a(1 - e^{-T}) + KTe^{-T} \int_0^1 e^{\theta T}(s_T(\theta + \phi_2))d\theta. \tag{4}$$

Equation (4) follows from the fact that cell 1 fires again at time T.

Similarly, cell 2 fires at $t = -\phi_2 T$ and $t = (1 - \phi_2)T$. It follows that

$$x_2((1 - \phi_2)T) = 1 = a(1 - e^{-T}) + KTe^{-T} \int_0^1 e^{\theta T}(s_T(\theta - \phi_2))d\theta. \tag{5}$$

Equations (4) and (5) determine both the period T and the phase difference ϕ_2. Subtracting (4) from (5) and dividing by T gives the condition

$$Ke^{-T}\int_0^1 e^{\theta T}\left(s_T(\theta+\phi_2)-s_T(\theta-\phi_2)\right)d\theta=0.$$

We are thus motivated to define the following function G, of which we want to find the zero solutions [34].

$$G(\phi_2)=Ke^{-T}\int_0^1 e^{\theta T}\left(s_T(\theta+\phi_2)-s_T(\theta-\phi_2)\right)d\theta. \tag{6}$$

Clearly, $\phi_2=0$ (and equivalently, $\phi_2=1$) is a solution. And because $s_T(\theta+1/2)=s_T(\theta-1/2)$, $\phi_2=1/2$ is also a solution. These solutions correspond to synchronous and anti-synchronous firing respectively. The sign of $G'(\phi_2)$ determines stability, where the prime signifies differentiation with respect to ϕ_2. $G'(\phi_2)>0$ corresponds to a stable solution; $G'(\phi_2)<0$ corresponds to an unstable solution; and $G'(\phi_2)=0$ indicates a bifurcation.

The function $G(\phi_2)$ is plotted in Figure 10 for three different values of α in the case of excitatory coupling. When $\alpha=4$, there are three solutions at $\phi_2=0,1/2$ and 1, but only the anti-synchronous solution is stable. At $\alpha=5.57$, a pitchfork bifurcation is born at $\phi_2=1/2$ and two additional stable solutions arise. These two additional stable solutions move towards $\phi_2=0$ and $\phi_2=1$ as α increases, shown for $\alpha=6$. In Figure 11, we have plotted the inhibitory case; the same set of solutions exist, but the stability is reversed.

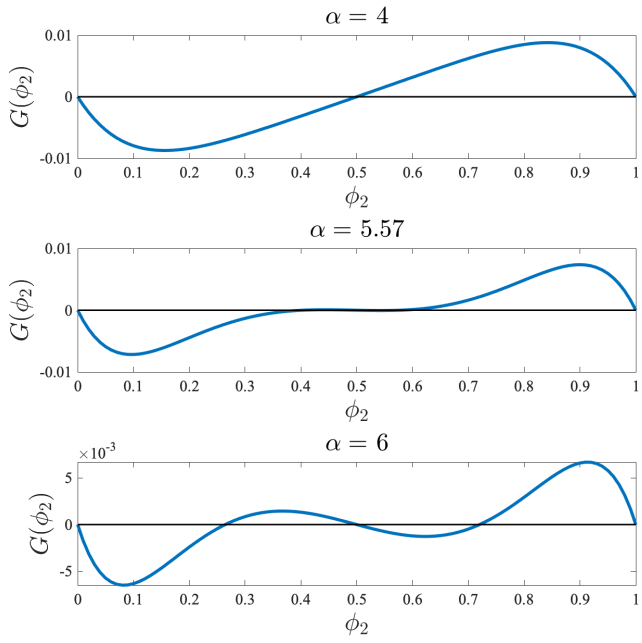

Figure 10: G plotted as a function of ϕ_2 for excitatory coupling, with three different values of α shown.

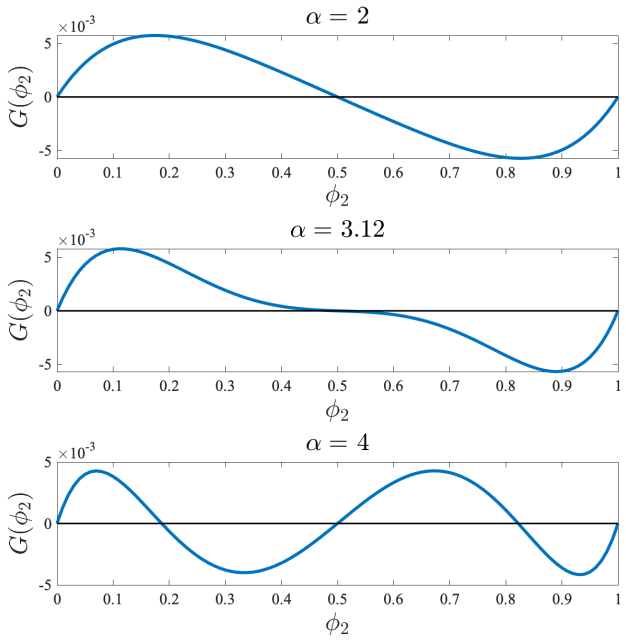

Figure 11: G plotted as a function of ϕ_2 for inhibitory coupling, with three different values of α shown.

4.2 Three-Cell Systems

We now extend the work in Section 4.1 to a three-cell system. By assuming cell 1 fires periodically at t_{s_1} which is of the form $nT = \{\dots, -T, 0, T, \dots\}$, cell 2 fires periodically at $t_{s_2} = (n - \phi_2)T$, and that cell 3 fires periodically at $t_{s_3} = (n - \phi_3)T$ with $n \in \mathbb{N}$, we can derive a set of three equations very similar to (4) and (5):

$$x_1(T) = 1 = a(1 - e^{-T}) + KTe^{-T} \int_0^1 e^{\theta T} \left(s_T(\theta + \phi_2) + s_T(\theta + \phi_3)\right) d\theta. \tag{7}$$

$$x_2((1 - \phi_2)T) = 1 = a(1 - e^{-T}) + KTe^{-T} \int_0^1 e^{\theta T} (s_T(\theta - \phi_2) + s_T(\theta - \phi_2 + \phi_3)) d\theta. \tag{8}$$

$$x_3((1 - \phi_3)T) = 1 = a(1 - e^{-T}) + KTe^{-T} \int_0^1 e^{\theta T} \left(s_T(\theta - \phi_3) + s_T(\theta + \phi_2 - \phi_3)\right) d\theta. \tag{9}$$

Similar to that of the two-cell case, these three equations determine both the period T and the phase differences
ϕ_2 and ϕ_3. Subtracting (8) from (7) and dividing by T gives the condition

$$Ke^{-T} \int_0^1 e^{\theta T} \left(s_T(\theta + \phi_2) + s_T(\theta + \phi_3) - s_T(\theta - \phi_2) - s_T(\theta - \phi_2 + \phi_3)\right) d\theta = 0.$$

As in the two-cell case, we are motivated to define the following function G_1:

$$G_1(\phi_2, \phi_3) = Ke^{-T} \int_0^1 e^{\theta T} \left(s_T(\theta + \phi_2) + s_T(\theta + \phi_3) - s_T(\theta - \phi_2) - s_T(\theta - \phi_2 + \phi_3)\right) d\theta. \tag{10}$$

Similarly, subtracting (9) from (7) and dividing by T gives the condition

$$Ke^{-T} \int_0^1 e^{\theta T} (s_T(\theta + \phi_2) + s_T(\theta + \phi_3) - s_T(\theta - \phi_3) - s_T(\theta + \phi_2 - \phi_3)) d\theta = 0.$$

We then define the function G_2:

$$G_2(\phi_2, \phi_3) = Ke^{-T} \int_0^1 e^{\theta T} (s_T(\theta + \phi_2) + s_T(\theta + \phi_3) - s_T(\theta - \phi_3) - s_T(\theta + \phi_2 - \phi_3)) d\theta = 0. \tag{11}$$

We want to find all pairs (ϕ_2, ϕ_3) that are zero solutions of G_1 and G_2, which represent the eventual phases that the system will become locked into. Clearly, the splay state solution $(2/3, 1/3)$ is a solution because:

$$G_1(2/3, 1/3) = Ke^{-T} \int_0^1 e^{\theta T} \left(s_T(\theta + 2/3) + s_T(\theta + 1/3) - s_T(\theta - 2/3) - s_T(\theta - 1/3)\right) d\theta = 0$$

and $G_2(2/3, 1/3) = Ke^{-T} \int_0^1 e^{\theta T} \left(s_T(\theta + 2/3) + s_T(\theta + 1/3) - s_T(\theta - 1/3) - s_T(\theta + 1/3)\right) d\theta = 0.$

Note that $(1/3, 2/3)$ also corresponds to the splay state solution and thus is a zero solution to G_1 and G_2 as well, but we focus on initial conditions in the fundamental domain defined by (3).

In Figures 12 - 15, we have created surfaces of G_1 and G_2 for both inhibitory and excitatory coupling, on which are interposed the Poincaré map trajectories. As in Section 3, the trajectories start at red and then flows towards orange, yellow, and so on.

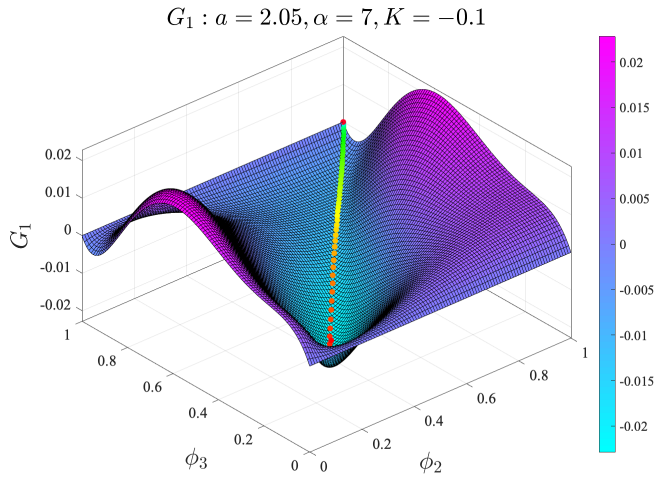

Figure 12: G_1 plotted as a function of phase differences ϕ_2 and ϕ_3 for inhibitory coupling. The Poincaré map trajectory interposed onto the surface, and color indicates the direction of time — beginning with red, then orange, and so on.

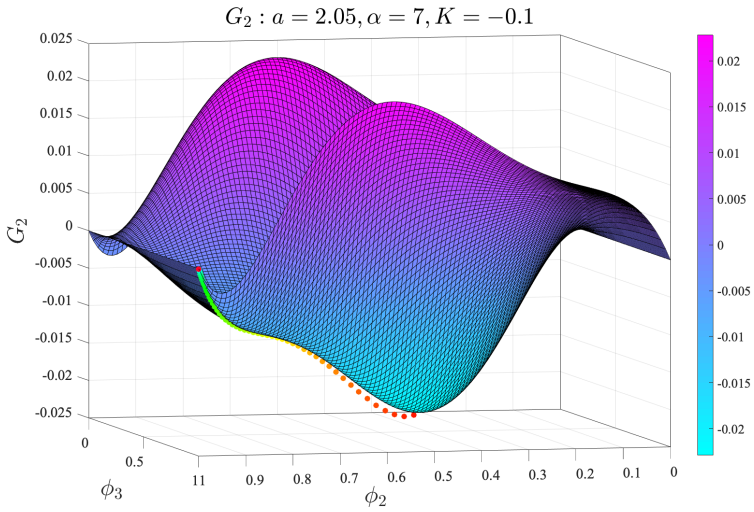

Figure 13: G_2 plotted as a function of phase differences ϕ_2 and ϕ_3 for inhibitory coupling. Poincaré map trajectory interposed on top, with same color-coding as Figure 12.

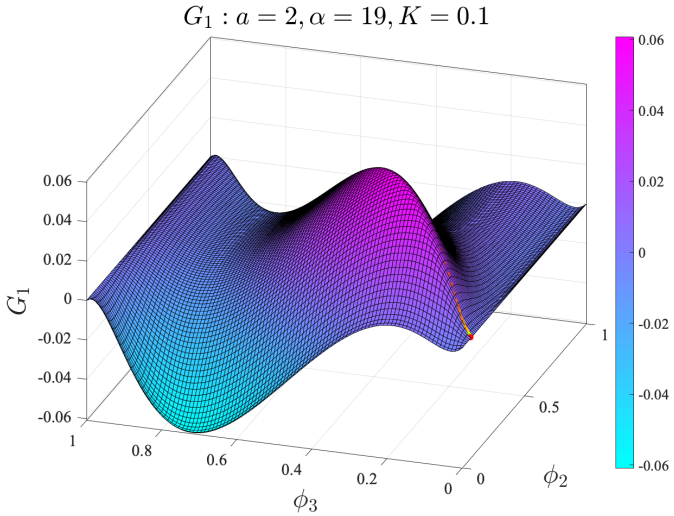

Figure 14: G_1 plotted as a function of phase differences ϕ_2 and ϕ_3 for excitatory coupling. Poincaré map trajectory interposed on top, with same color-coding as Figure 12.

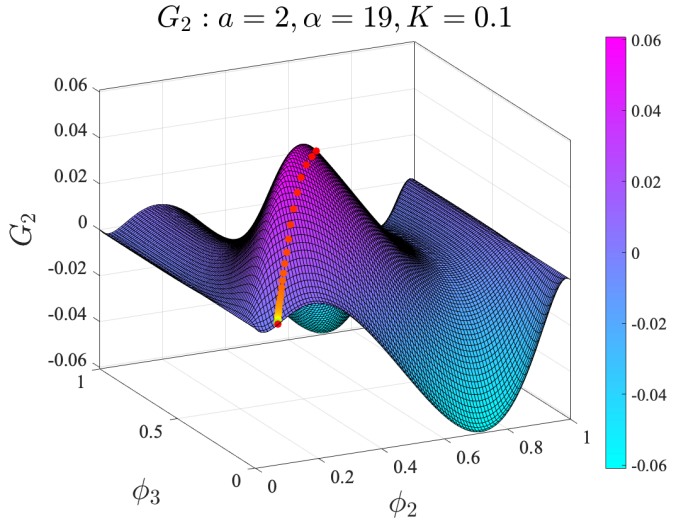

Figure 15: G_2 plotted as a function of phase differences ϕ_2 and ϕ_3 for excitatory coupling. Poincaré map trajectory interposed on top, with same color-coding as Figure 12.

The trajectories in Figures 12 - 15 end at coordinates (ϕ_2, ϕ_3) where $G_1 = G_2 = 0$, as expected. We also note that the trajectories follow the direction of the gradient, which aligns with the conclusions outlined in Section 4.1. The trajectories in Figures 12 - 13 are attracted towards the full synchrony state. In contrast, the trajectories in Figures 14 - 15 are attracted towards a 2-1 cluster synchrony state.

As a final note, we observe the final point of each trajectory aligns perfectly with the surfaces of G_1 and G_2, indicating that our theoretical predictions and numerical simulations support one another.

4.3 Higher Order Systems

We can extend the G-functions presented in Sections 4.1 and 4.2 to describe the phase-locked dynamics of higher order systems.

For a general N-cell neural network, assume that cell N is separated from cell 1 by a phase difference of ϕ_N as in
Figure 9. Following a similar derivation procedure as that of sections 4.1 and 4.2, we find that there will be $N-1$ G-functions that we want to find the zero solutions of. The Mth G-function, where $1 \leq M < N$, has the form

$$G_M(\phi_2, \phi_3, ..., \phi_N) = Ke^{-T} \int_0^1 e^{\theta T} \left(\sum_{k=2}^{N} s_T(\theta + \phi_k) - s_T(\theta - \phi_{M+1}) - \sum_{k=2}^{N} s_T(\theta + \phi_k - \phi_{M+1}) \right) d\theta = 0.$$

As in Section 4.2, a solution's stability is again determined by the sign of the gradient.

5 Dynamics of Small Networks with Different Symmetries and Connectivities

In this section, we describe the dynamics of Poincaré maps as a function of the parameter α. This section centers on three-cell and four-cell systems with different coupling matrices. Our results are based on precise numerical simulations for fixed finite coupling strength K and fixed a.

5.1 All-to-All Coupling

5.1.1 Three-Cell System

We start by reviewing the dynamics of three identical all-to-all coupled oscillators, studied in [29] with very small coupling strengths $K \to 0$. Although [29] uses a perturbative method with $K = \pm 0.01$, we use numerical simulations to observe the same sequence of attractor states as a function of α.

We first review inhibitory coupling. For very small α, the system falls into a 2-1 cluster synchrony. As α increases, we observe both 2-1 cluster synchrony solutions and full synchrony solutions. Finally, for large α, we can observe full synchrony, 2-1 cluster synchrony, and the splay state solution.

We next consider excitatory coupling. For small α, the system can fall into a splay state or a 2-1 cluster synchrony. Upon increasing α, the splay state solution undergoes a Hopf bifurcation, becoming a limit cycle. And as α increases further, the system bifurcates again and falls into either a 2-1 cluster synchrony or a full synchrony.

Figure 16 shows the basin of attraction for these solution states given fixed parameters of a, α, and K. We obtain these results by integrating the system from a large set of varying initial conditions

and determining the eventual solution state. As in Section 3, we use initial conditions in which $x_1 \leq x_2 \leq x_3 \leq 1$. Each colored square in Figure 16 represents a different initial condition. From the top sub-figure that shows inhibitory coupling, we see that the splay state has the largest basin of attraction. In the bottom sub-figure showing excitatory coupling, the limit cycle solution has the largest basin of attraction.

For both inhibitory and excitatory coupling and different values of α, Figure 17 shows the size of basin of attraction of different solution states represented as normalized area. We can estimate the probability of observing a given solution state. For instance, in excitatory coupling, the full synchrony solution has a very small basin of attraction compared to the other solution states.

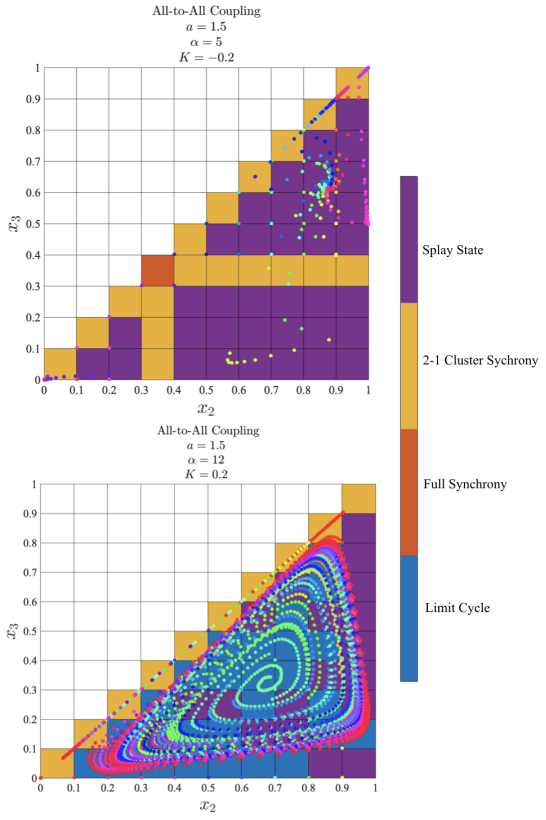

Figure 16: Basin of Attraction.
Top: $a = 1.5, \alpha = 5, K = -0.2$.
Bottom: $a = 1.5, \alpha = 12, K = 0.2$.

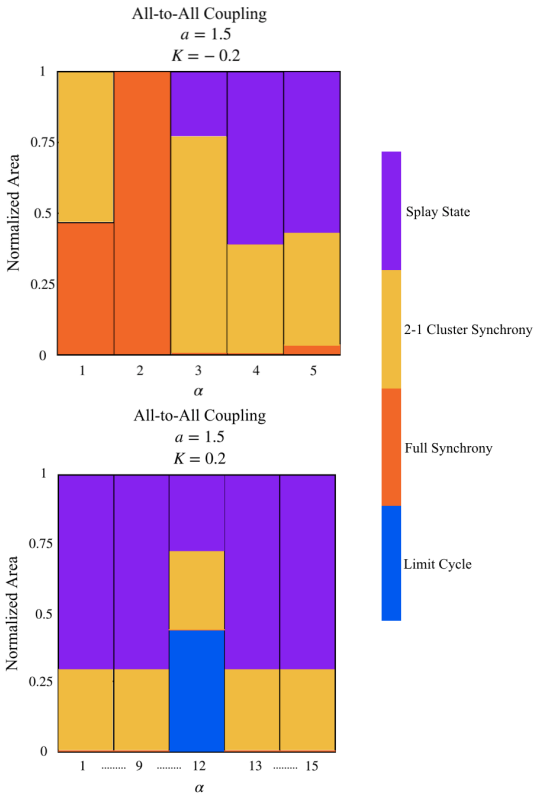

Figure 17: Basin of attraction of different solution states represented as a function of α.

5.1.2 Four-Cell System

We now review the dynamics of four identical all-to-all coupled oscillators. The sequence of solutions is very similar to that of the three-cell case, but we observe a richer set of attractors.

We first analyze inhibitory coupling, with $K = -0.2$. The sequence of attractor states is shown in Figures 18 and 19. For small α, the system is attracted towards full synchrony. As α increases, a saddle node on the $x_4 = 0$ face appears, an attracting direction normal to the face and repelling direction along the edge towards full synchrony. As α further increases, the solution state becomes a 2-2 cluster synchrony, and the saddle node becomes an attractor. Finally, for larger values of α, the system falls into a stable splay state.

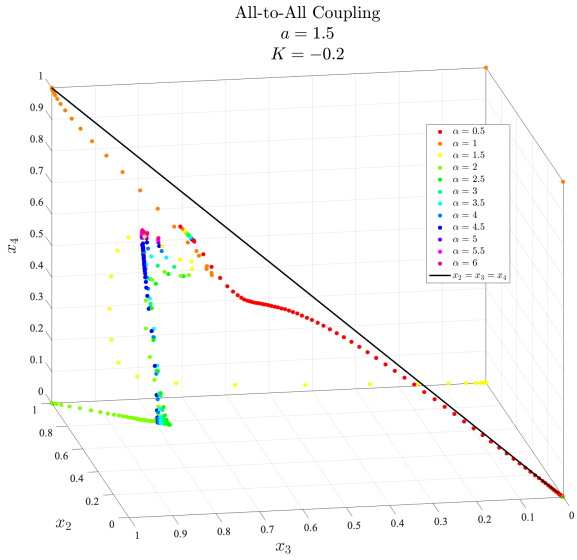

Figure 18: The Poincaré maps plotted for $\alpha = 0.5 - 6$, displaying the progression from full synchrony to 2-2 cluster states to splay states.

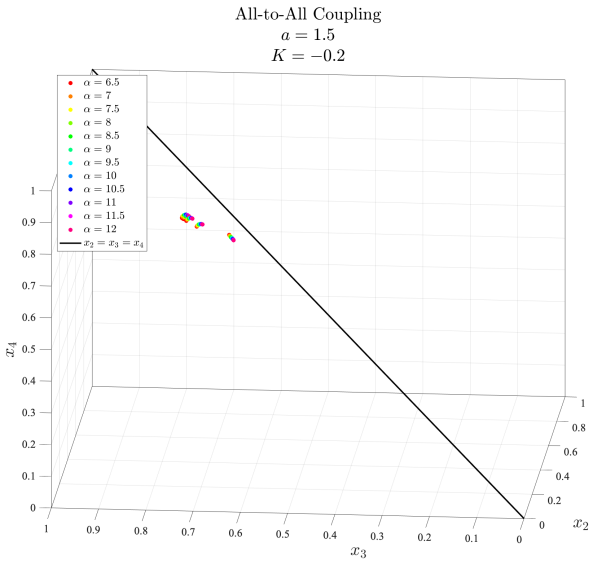

Figure 19: The Poincaré maps plotted for $\alpha = 6.5 - 12$, displaying the stable splay state solution.

We now consider the excitatory case, simulated with $K = 0.2$. See Figures 20 and 21 for the sequence of attractor states. For small α, the system falls into a splay state. As α increases, the splay state bifurcates into a limit cycle. The limit cycle is attracting, and the size of the orbit increases with α. Up until a critical value of α_c, the limit cycle solution flows inward. Once α reaches α_c, the system bifurcates once again and the limit cycles flows outward. As α increases further, the limit cycle falls onto the boundary of the cube and breaks down, shown in Figure 20 at $\alpha = 24.5$. After this point, we observe both the 2-1-1 cluster states for smaller values of α and 3-1 cluster states for larger values of α.

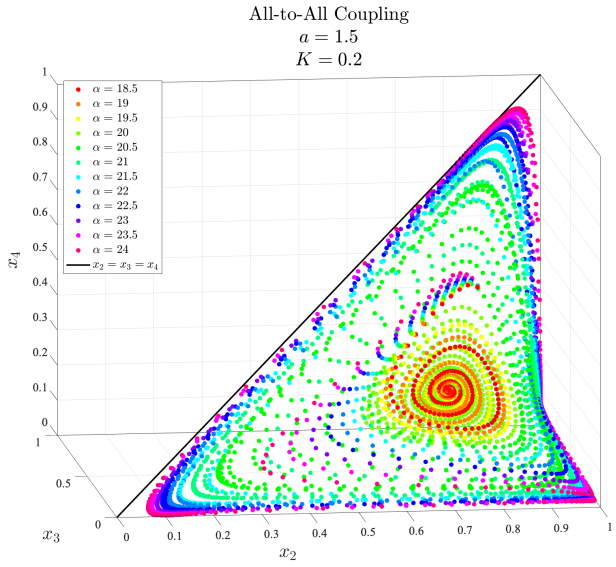

Figure 20: The Poincaré maps plotted for $\alpha = 18.5 - 24$, showcasing the limit cycle solution.

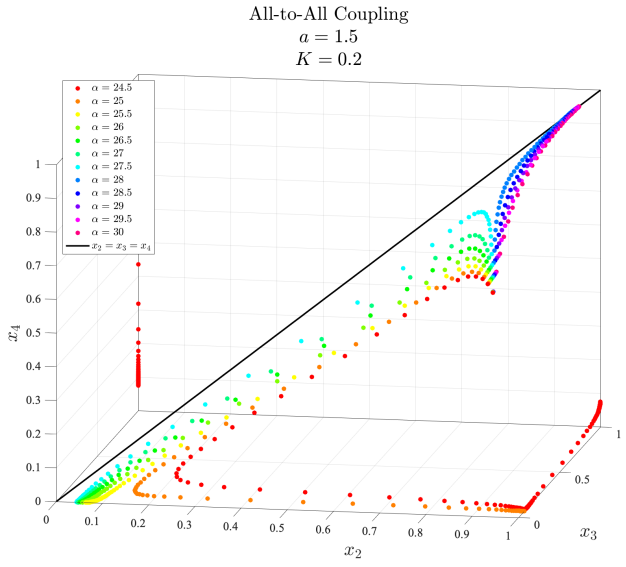

Figure 21: The Poincaré maps plotted for $\alpha = 24.5 - 30$, displaying the breakdown of the limit cycle solution.

5.2 Star Network Coupling

In this section, we discuss the rich dynamics of star network coupled systems of 4 cells. We first examine how the unique structure of the coupling matrix can generally affect the dynamics. We then describe the dynamics of inhibitory and excitatory-coupled systems in greater detail, focusing on the rich patterns and symmetries as a function of α. We will refer to the central oscillator as cell 4, to which cells 1, 2, and 3 are each coupled with.

5.2.1 General Discussion

First, with inhibitory coupling, cell 4 can be so strongly inhibited that it fires far fewer times than the other cells in the network. In fact, for small enough values of α, we may observe an oscillation death of cell 4. We therefore use cell 1 to generate the Poincaré maps shown in Figure 22. In contrast, with excitatory coupling, cell 4 can be so strongly excited that it fires many more times than the other cells in the network. We therefore use cell 4 to generate the Poincaré maps in Figure 23. These dynamics are studied in greater detail in Section 5.2.2.

Second, as noted in Section 1, the symmetry of connectivity can provide a guidance in determining the final solution state. In Figures 22 and 23, we have plotted the Poincaré maps of inhibitory and excitatory coupled systems with three different connectivity matrices.

The top sub-figures are generated with a coupling matrix A of the form

$$A = K \begin{pmatrix} 0 & 0 & 0 & 1 \\ 0 & 0 & 0 & 1 \\ 0 & 0 & 0 & 1 \\ 1/3 & 1/3 & 1/3 & 0 \end{pmatrix} \tag{12}$$

where $K = -0.2$ in Figure 22 and $K = 0.2$ in Figure 23. The motivation behind this coupling matrix is to ensure that the collective input from cells 1-3 to cell 4 is the same as the input from cell 4 to each of those three cells. We observe that the dynamics behave similar to that of the all-to-all case: full synchrony for inhibitory coupling and a splay state (close to 3-1 cluster synchrony) for excitatory coupling.

The middle sub-figures are generated with a coupling matrix A of the form

$$A = K \begin{pmatrix} 0 & 0 & 0 & 1 \\ 0 & 0 & 0 & 1 \\ 0 & 0 & 0 & 1 \\ 2/3 & 2/3 & 2/3 & 0 \end{pmatrix} \tag{13}$$

with the aforementioned K values. With this coupling matrix, the collective input from cells 1-3 to cell 4 is twice the amount of input from cell 4 to each of the other three cells. We observe that this increase in synaptic input causes the system to bifurcate, resulting in the unique trajectories showcased. The inhibited system's rich dynamics are a result of cells 1, 2, 3 forming a limit cycle while cell 4 fires slowly. Similarly, in the excited system, cells 1, 2, 3 form a limit cycle while cell 4 fires very rapidly.

The bottom sub-figures are generated with a coupling matrix A of the form

$$A = K \begin{pmatrix} 0 & 0 & 0 & 1 \\ 0 & 0 & 0 & 1 \\ 0 & 0 & 0 & 1 \\ 1 & 1 & 1 & 0 \end{pmatrix} \tag{14}$$

with the same K values as before. Here, the collective input from cells 1-3 to cell 4 is three times the amount of input from cell 4 to each of the other cells. This increase in synaptic input causes the

inhibited system to bifurcate again, resulting in a new solution state: the death of an oscillator. In contrast, the excited system does not bifurcate again; cells 1-3 remain in a limit cycle while cell 4 fires very rapidly.

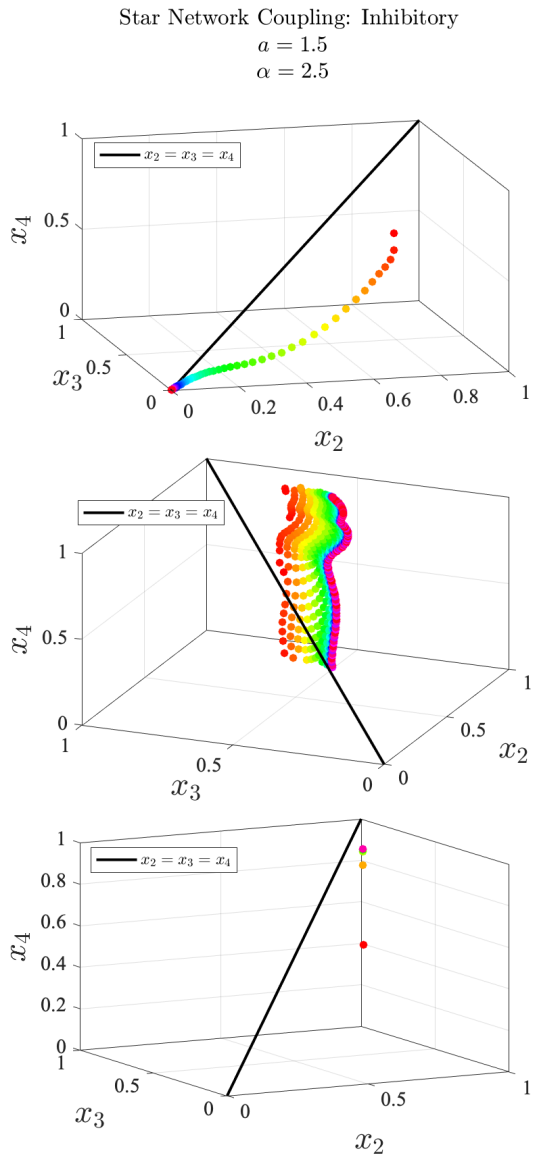

Figure 22: Poincaré maps plotted for inhibitory coupling, with three different connectivity matrices.

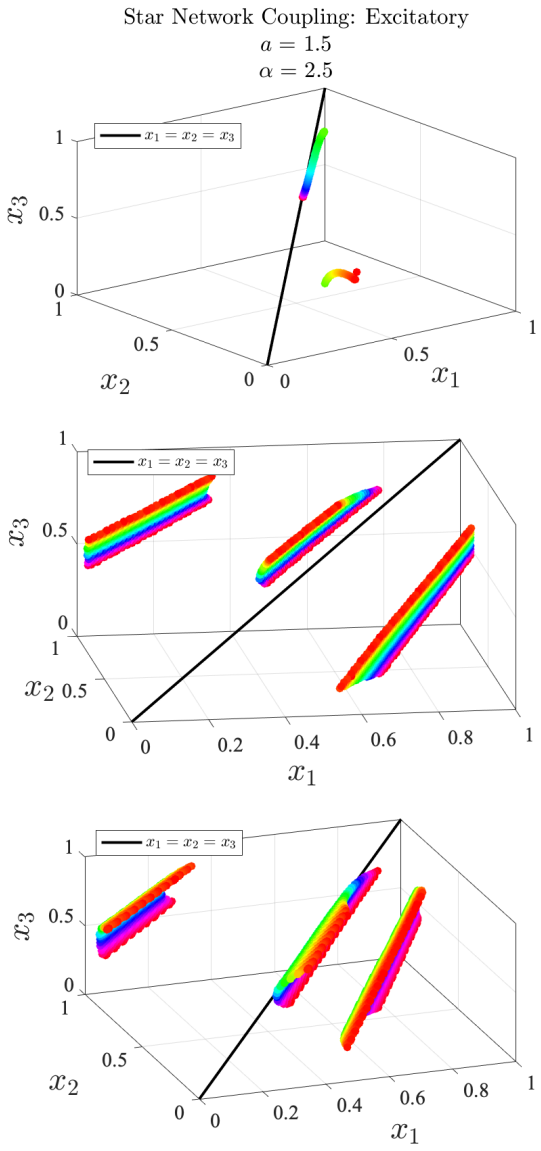

Figure 23: Poincaré maps plotted for excitatory coupling, with three different connectivity matrices.

5.2.2 Uniform Star Network Coupled Systems

In this section, we comprehensively describe the dynamics of star network coupled four-cell system with uniform coupling; i.e. the coupling matrix is of the form in (14).

For both inhibitory and excitatory coupling, the phase diagram of attractor states as a function of α in schematically shown in Figure 24.

We first examine inhibitory coupling. As noted in Section 5.2.1, for small α, we observe an oscillation death of the central oscillator. From Figure 25, we see that this phenomenon is a result

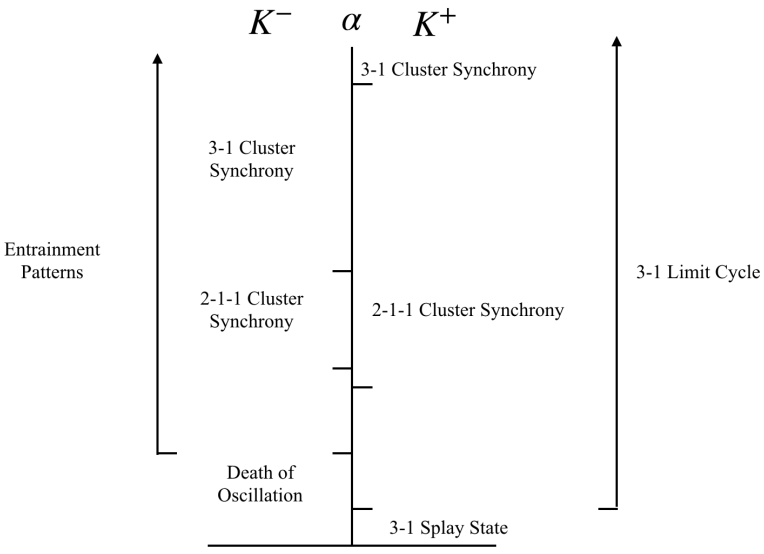

Figure 24: Schematic phase diagram of attractor states as a function of α.

of the strong inhibition. Specifically, cells 1, 2, and 3 inhibit the central oscillator so strongly that that it is prevented from firing and

$$\lim_{t\to\infty} s_4 = 0.$$

Increasing α revives cell 4 and the systems forms entrainment patterns, in which cells 1, 2, and 3 fire several times before cell 4 fires. Figure 26 shows a such entrainment pattern, where cells 1-3 collectively fire six times before cell 4 fires. Upon increasing α even further, the system bifurcates and cluster synchrony states are born. We observe stable 2-1-1 cluster synchrony states for intermediate range of α and 3-1 cluster synchrony states for large α.

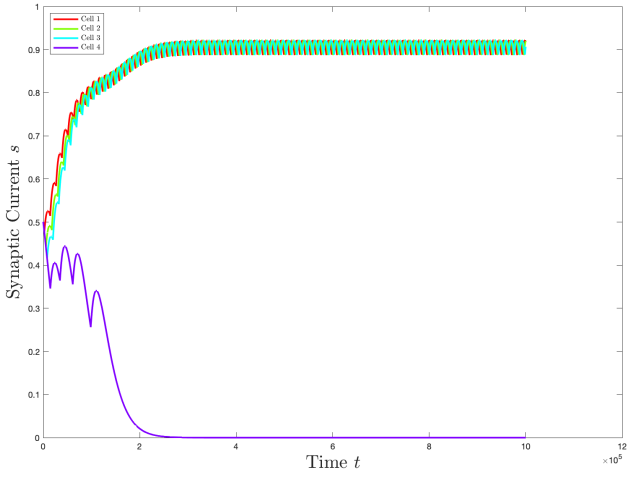

Figure 25: Plot of the synaptic currents s, simulated with $K = -0.2, a = 1.5$, and $\alpha = 0.5$. Shows the death of oscillation of cell 4.

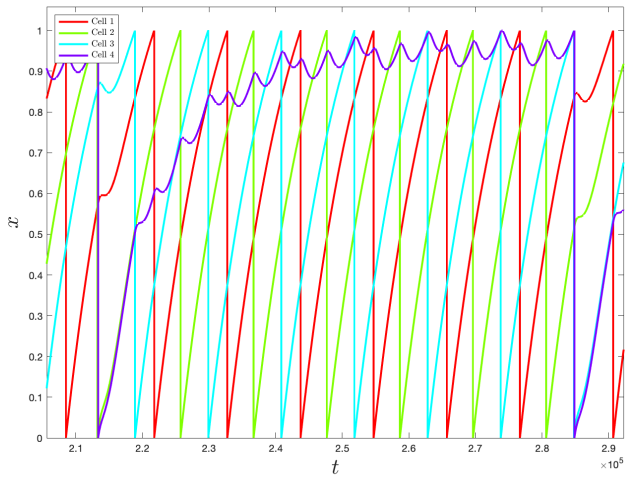

Figure 26: Plot of the action potentials x, simulated with $K = -0.2, a = 1.5$, and $\alpha = 12.5$. Illustrates entrainment patterns.

We next examine excitatory coupling. These dynamics are particularly rich, as the solutions are time-evolving. For small α, cells 1, 2, and 3 will form a splay state, while cell 4 fires rapidly. We call this phenomenon a "3-1 splay state," shown in Figure 27. Then, at some critical α_c, the system bifurcates and cells 1, 2, and 3 form a limit cycle – similar to the all-to-all case. However, changing the connectivity from all-to-all to star network gives rise to many interesting patterns. For instance, we may observe behaviors similar to the limit cycle in the all-to-all coupled case, shown in Figure 28. It is also possible for these three cells to synchronize while remaining in limit cycle, due to uniqueness of the connectivity matrix. For large α, we observe stable 2-1-1 cluster synchrony states, where the synchronized cluster is any two of the cells 1, 2, and 3. And for very large α, we observe 3-1 cluster synchrony states, where cells 1, 2, and 3 are synchronized.

The color of the points in Figures 27 and 28 shows that excitatory-coupled star networks falls into quasi-periodic patterns. The identical colors in the different pieces of the trajectories indicate that the system periodically traverses each part of the trajectories.

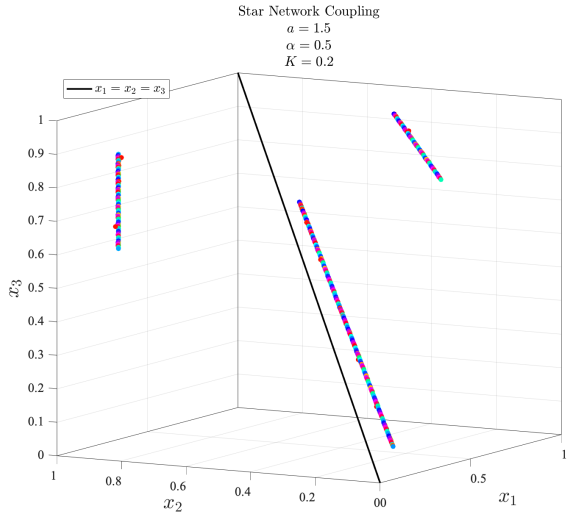

Figure 27: 3-1 Splay state solution in a star network. Here, cells 1, 2, and 3 form a splay state while cell 4 fires rapidly, corresponding to straight lines.

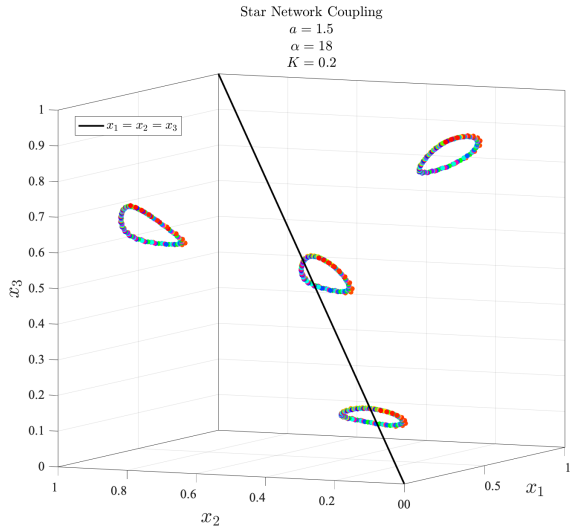

Figure 28: 3-1 Limit cycle solution in a star network. Cells 1, 2, and 3 form a limit cycle while cell 4 fires rapidly.

6 Discussion

We have systematically studied the dynamics of the reduced state space via Poincaré maps for both all-to-all coupled and star-like networks. In Section 4, we developed a set of analytic functions to describe the stability of phase-locked states. The behavior of our derived equations aligns with the results of numerical simulations. And in Section 5, we thoroughly explored the rich patterns exhibited in a star network, revealing novel states unobserved in the all-to-all network: the death of oscillation for slow and inhibitory synapses and a quasi-periodic pattern for fast and excitatory synapses.

One direction for future research is to extend the work in Section 4 to star networks. The proofs of Section 4 depends on the assumption of a phase-locked system. However, as we have seen in Section 5.2.2, while the dynamics of a star-like network are periodic, they are also much more complex than that of an all-to-all network. One potential approach to extend Section 4 to inhibitory-coupled star networks is to use the entrainment patterns: if we know how many times cells 1, 2, and 3 collectively fire before cell 4 fires, we may be able to derive equations similar to (4) - (5) and (7) - (9).

Another direction for future research is to further clarify the role that connectivity plays in system dynamics. As we noted in Sections 1 and 5.2.1, connectivity and strength of coupling clearly affects system dynamics. After all, as we saw in Figures 22 and 23, increasing the coupling strength between the central cell and other cells in the system causes an inhibited system to progress from full synchrony to oscillation death and an excited system to progress from a stable splay state to time-evolving solutions. In the future, we hope to further elucidate this sequence of bifurcations.

In the continuum limit ($N \to \infty$), the conventional approach of studying its dynamics is a mean-field approach by defining an "order parameter" that is a weighted average of all oscillators' configuration. Many efforts focus on the stability of the fully synchronized states and the fully asynchronous splay states. However, many real systems [6, 35] have finite number of cells ($N \sim 10^1$). The mean-field approach breaks down due to strong temporal fluctuations. As we have seen in this paper, the overall picture of attractors for small N is much richer than a competition between sync and splay. Therefore, our results shed lights on connecting symmetries and patterns in dynamical systems with finite degrees of freedom.

A recent experiment [35] on chemical oscillators and the Belousov-Zhabotinsky (BZ) reaction in star networks demonstrates intriguing temporal phase-locking phenomena. The essential BZ reaction can be reduced to a four-dimensional model [36] that mimics periodic surges in chemical concentrations like spikes. Thus, our analysis may clarify understanding of not only neural circuits but also of other pulse-coupled oscillator systems.

7 Acknowledgements

I sincerely thank my mentor, Dr. Bolun Chen of Brandeis University, for suggesting this project and providing me thorough and invaluable guidance and advice. I am also grateful to Yongyi Chen and Dr. Tanya Khovanova for reviewing drafts and offering helpful comments. Finally, I would to thank the MIT PRIMES program, particularly Prof. Pavel Etingof and Dr. Slava Gerovitch, for giving me this research opportunity.

References

[1] John Buck. Synchronous rhythmic flashing of fireflies. ii. *The Quarterly review of biology*, 63(3):265–289, 1988.

[2] Charles S. Peskin. Mathematical aspects of heart physiology. 1975.

[3] AE Dolbear. The cricket as a thermometer. *The American Naturalist*, 31(371):970–971, 1897.

[4] Andrea Ravignani, Daniel L Bowling, and W Fitch. Chorusing, synchrony, and the evolutionary functions of rhythm. *Frontiers in psychology*, 5:1118, 2014.

[5] Eve Marder and Ronald L Calabrese. Principles of rhythmic motor pattern generation. *Physiological reviews*, 76(3):687–717, 1996.

[6] Eve Marder and Dirk Bucher. Central pattern generators and the control of rhythmic movements. *Current biology*, 11(23):R986–R996, 2001.

[7] Lauren M Jones, Alfredo Fontanini, Brian F Sadacca, Paul Miller, and Donald B Katz. Natural stimuli evoke dynamic sequences of states in sensory cortical ensembles. *Proceedings of the National Academy of Sciences*, 104(47):18772–18777, 2007.

[8] Margaret F Carr, Shantanu P Jadhav, and Loren M Frank. Hippocampal replay in the awake state: a potential substrate for memory consolidation and retrieval. *Nature neuroscience*, 14(2):147, 2011.

[9] Paul Miller and Donald B Katz. Stochastic transitions between neural states in taste processing and decision-making. *Journal of Neuroscience*, 30(7):2559–2570, 2010.

[10] Wolfgang Maass and Henry Markram. On the computational power of circuits of spiking neurons. *Journal of computer and system sciences*, 69(4):593–616, 2004.

[11] Samanwoy Ghosh-Dastidar and Hojjat Adeli. Spiking neural networks. *International journal of neural systems*, 19(04):295–308, 2009.

[12] Hélene Paugam-Moisy and Sander Bohte. Computing with spiking neuron networks. *Handbook of natural computing*, pages 335–376, 2012.

[13] David Daniel Cox and Thomas Dean. Neural networks and neuroscience-inspired computer vision. *Current Biology*, 24(18):R921–R929, 2014.

[14] Adam H Marblestone, Greg Wayne, and Konrad P Kording. Toward an integration of deep learning and neuroscience. *Frontiers in computational neuroscience*, 10:94, 2016.

[15] Stephen J Verzi, Fredrick Rothganger, Ojas D Parekh, Tu-Thach Quach, Nadine E Miner, Craig M Vineyard, Conrad D James, and James B Aimone. Computing with spikes: The advantage of fine-grained timing. *Neural computation*, 30(10):2660–2690, 2018.

[16] Terrence J Sejnowski. *The deep learning revolution*. 2018.

[17] Eugene M Izhikevich. Simple model of spiking neurons. *IEEE Transactions on neural networks*, 14(6):1569–1572, 2003.

[18] Arkady Pikovsky, Jurgen Kurths, Michael Rosenblum, and Jürgen Kurths. *Synchronization: a universal concept in nonlinear sciences*, volume 12. Cambridge university press, 2003.

[19] Peter Ashwin, Stephen Coombes, and Rachel Nicks. Mathematical frameworks for oscillatory network dynamics in neuroscience. *The Journal of Mathematical Neuroscience*, 6(1):2, 2016.

[20] James J Collins and Ian N Stewart. Coupled nonlinear oscillators and the symmetries of animal gaits. *Journal of Nonlinear Science*, 3(1):349–392, 1993.

[21] Martin Golubitsky and Ian Stewart. Patterns of oscillation in coupled cell systems. In *Geometry, mechanics, and dynamics*, pages 243–286. Springer, 2002.

[22] Martin Golubitsky and Ian Stewart. Nonlinear dynamics of networks: the groupoid formalism. *Bulletin of the american mathematical society*, 43(3):305–364, 2006.

[23] Martin Golubitsky, Ian Stewart, and David G Schaeffer. *Singularities and groups in bifurcation theory*, volume 2. Springer Science & Business Media, 2012.

[24] Vincenzo Nicosia, Miguel Valencia, Mario Chavez, Albert Díaz-Guilera, and Vito Latora. Remote synchronization reveals network symmetries and functional modules. *Physical review letters*, 110(17):174102, 2013.

[25] Louis M Pecora, Francesco Sorrentino, Aaron M Hagerstrom, Thomas E Murphy, and Rajarshi Roy. Cluster synchronization and isolated desynchronization in complex networks with symmetries. *Nature communications*, 5:4079, 2014.

[26] Francesco Sorrentino, Louis M Pecora, Aaron M Hagerstrom, Thomas E Murphy, and Rajarshi Roy. Complete characterization of the stability of cluster synchronization in complex dynamical networks. *Science advances*, 2(4):e1501737, 2016.

[27] Renato E Mirollo and Steven H Strogatz. Synchronization of pulse-coupled biological oscillators. *SIAM Journal on Applied Mathematics*, 50(6):1645–1662, 1990.

[28] LF Abbott and Carl van Vreeswijk. Asynchronous states in networks of pulse-coupled oscillators. *Physical Review E*, 48(2):1483, 1993.

[29] Bolun Chen, Jan R. Engelbrecht, and Renato Mirollo. Cluster synchronization in networks of identical oscillators with α-function pulse coupling. *Phys. Rev. E*, 95:022207, Feb 2017.

[30] Rüdiger Zillmer, Roberto Livi, Antonio Politi, and Alessandro Torcini. Stability of the splay state in pulse-coupled networks. *Phys. Rev. E*, 76:046102, Oct 2007.

[31] Can Xu, Jian Gao, Stefano Boccaletti, Zhigang Zheng, and Shuguang Guan. Synchronization in starlike networks of phase oscillators. *Physical Review E*, 100(1):012212, 2019.

[32] Lawrence G Roberts and Barry D Wessler. Computer network development to achieve resource sharing. In *Proceedings of the May 5-7, 1970, spring joint computer conference*, pages 543–549. ACM, 1970.

[33] Yu Hu, Steven L Brunton, Nicholas Cain, Stefan Mihalas, J Nathan Kutz, and Eric Shea-Brown. Feedback through graph motifs relates structure and function in complex networks. *Physical Review E*, 98(6):062312, 2018.

[34] Carl Van Vreeswijk, L. F. Abbott, and G. Bard Ermentrout. When inhibition not excitation synchronizes neural firing. *Journal of Computational Neuroscience*, 1(4):313–321, Dec 1994.

[35] Michael M Norton, Nathan Tompkins, Baptiste Blanc, Matthew C Cambria, Jesse Held, and Seth Fraden. Dynamics of reaction-diffusion oscillators in star networks. *arXiv preprint arXiv:1907.03924*, 2019.

[36] Vladimir K Vanag and Irving R Epstein. Pattern formation in a tunable medium: The belousov-zhabotinsky reaction in an aerosol ot microemulsion. *Physical review letters*, 87(22):228301, 2001.